Plastic crystal phases of simple water models

J. L. Aragones and C. Vega[a)]
Dpto. de Química Física, Facultad de Ciencias Químicas, Universidad Complutense, 28040 Madrid, Spain

(Received 16 March 2009; accepted 1 June 2009; published online 26 June 2009)

We report the appearance of two plastic crystal phases of water at high pressure and temperature using computer simulations. In one of them the oxygen atoms form a body centered cubic structure (bcc) and in the other they form a face centered cubic structure (fcc). In both cases the water molecules were able to rotate almost freely. We have found that the bcc plastic crystal transformed into a fcc plastic crystal via a Martensitic phase transition when heated at constant pressure. We have performed the characterization and localization in the phase diagram of these plastic crystal phases for the SPC/E, TIP4P, and TIP4P/2005 water potential models. For TIP4P/2005 model free energy calculations were carried out for the bcc plastic crystal and fcc plastic crystal using a new method (which is a slight variation of the Einstein crystal method) proposed for these types of solid. The initial coexistence points for the SPC/E and TIP4P models were obtained using Hamiltonian Gibbs–Duhem integration. For all of these models these two plastic crystal phases appear in the high pressure and temperature region of the phase diagram. It would be of interest to study if such plastic crystal phases do indeed exist for real water. This would shed some light on the question of whether these models can describe satisfactorily the high pressure part of the phase diagram of water, and if not, where and why they fail. © *2009 American Institute of Physics*. [DOI: 10.1063/1.3156856]

I. INTRODUCTION

The phase diagram of water, although relatively well known, is far from being complete. Besides ice Ih, other solid phases were found at the beginning[1–3] of the past century, toward the end[4] and even in this century.[5] The search of new solid phases has taken two principal routes. The first is the search (at low temperatures) for proton ordered analogous of the high temperature proton disordered ices. This is the research that lead to the discovery of ices VIII,[6] XI,[7] IX,[8] XIII,[5] and XIV (Ref. 5) (ice VI being probably the only proton disordered ice for which the proton ordered ice has not yet been found). The second route is the search of new ices at high pressures and/or temperatures. The discovery of ice VII, by Bridgmann[9] and the evidence of ice X (Ref. 10) illustrate the fact that new solid phases can be found under extreme pressures.[11–13] Notice that such extreme conditions may be found in other places within the solar system so this is of interest for the planetary sciences.[14] However, it must be recognized that performing experiments at high pressures is difficult, and so-far there is not a completely clear understanding of the aspect of the phase diagram of water at high pressures. Even the melting point curve of water at high pressures is a subject of current interest.[15–22] A quick look in Fig. 1 (where different experimental measurements of the melting curve of water at high pressures is presented) illustrates the fact that melting lines obtained by various groups are different, and that some consensus about what is happening in this region of the phase diagram of water is required.

Computer simulations of water started with a delay of about 60 years with respect to experiments, the first simulations of water appeared about 40 years ago.[23,24] At the beginning the interest focused on finding reasonable water models that allowed one to understand the physics of liquid water. The study of phase transitions in water by computer simulation started somewhat later. First the vapor-liquid equilibria was considered,[25–27] and more recently the study of fluid-solid and solid-solid equilibria.[28–34] Five years ago we presented for the first time the phase diagram of water as obtained from computer simulations,[34] for two water models, the SPC/E (Ref. 35) and the TIP4P (Ref. 36) models. It was shown that the TIP4P model was able to provide a reasonable description of the phase diagram of water. The main two defects of the model were that the melting points were too low, and that the freezing pressures were too high above the room temperature. We have since proposed a modified version of the TIP4P model, denoted as TIP4P/2005,[37] that improves the prediction of the melting point temperatures and provides an excellent description of the properties of water.[38] Initially we computed the low pressure region of the phase diagram for the TIP4P/2005 model, showing good agreement with experiment. Later on and motivated by the experimental work of Dolan *et al.*[39] showing that at 400 K and high pressures water freezes in a few nanoseconds, we performed computer simulation studies of the kinetics of freezing at these conditions. It was found[40] that water freezes very quickly in the simulations at these high pressures and temperatures, in clear contrast with the extremely long runs required to freeze water into ice Ih at low temperatures.[41–44] The surprise was that in the simulations water does not freeze into ice VII but into a new phase, which was a plastic crystal (PC).[40] In this PC phase the oxygens are located in a bcc arrangement (as in ice VII) but the molecules were able to rotate almost freely (i.e., a PC phase). This PC phase was also found by Takii *et al.*[45] for TIP5P, and for the TIP4P and

a)Electronic mail: cvega@quim.ucm.es.

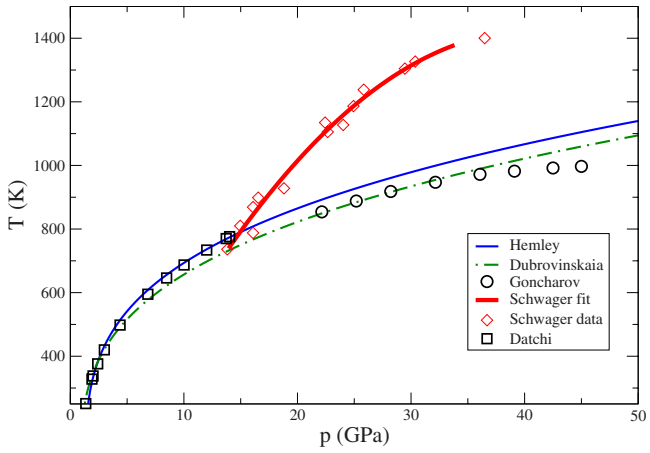

FIG. 1. (Color online) Experimental data for the melting curve of the ice VII. Reference 20: thick solid line and diamonds; Ref. 18: open squares; Ref. 17: thin solid line; Ref. 16: dashed-dotted line; Ref. 15: open circles.

SPC/E models. Therefore, it seems at this point necessary to recalculate the high pressure part of the phase diagram of TIP4P and SPC/E to include this new PC phase that was overlooked in our previous study.[34] This requires free energy calculations for the PC phase. In this work we shall describe in detail how to perform free energy calculations for these types of solid.

Another issue of interest is the layout of the phase diagram of these rigid water models (TIP4P, TIP4P/2005, and SPC/E) at extremely high pressures. In particular it would be of interest to establish if a solid with a fcc arrangement of the oxygens (i.e., a close packed structure) may appear for these models at extremely high pressures.[45] As will be shown, this is indeed the case. A PC phase with a fcc arrangement of the oxygens appears at high pressures and temperatures, allowing a better packing of the molecules than the typical bcc arrangement of ice VII or the bcc PC. These two PC phases (bcc and fcc) are also found for the TIP4P and SPC/E models so that they seem to be present in all water models. In these models water is described by a Lennard-Jones (LJ) center plus additional point charges. At high temperatures, the hydrogen bond energy (in k_BT units) is not sufficient to maintain the hydrogen bonding network and the molecules start to rotate. Once the importance of the charges is reduced, the relatively spherical shape of water makes the existence of a PC phase possible. PC phases are also found experimentally for slightly anisotropic molecules as N_2 or O_2.[46]

A word of caution is needed with respect to the conclusions of this work. Our main goal is to accurately determine the complete phase diagram of popular water models. Since these models are used in thousands of simulation studies it is important to know to what extent they can describe satisfactorily the phase diagram of water, and where and why they fail to do so. However, it should be clearly pointed out that SPC/E, TIP4P, and TIP4P/2005 are rigid models and they cannot describe properly the formation or the breaking of chemical bonds. For this reason these models are completely useless when it comes to understanding the formation of ice X. In ice X, the oxygens form a bcc lattice and the hydrogens are located in the middle of the O–O bonds. Also, at extremely high temperatures a superionic solid has been proposed[47] (where the oxygens form a lattice and the hydrogens diffuse within the oxygen network). The rigid models of this work cannot describe these situations. Obviously only first principle calculations can do that.[47,48] Rather the phase diagram presented here corresponds to what approximately would occur in the phase diagram of water in the absence of deformation or breaking of chemical bonds. It will be shown that for these models, water adopts close packed structures at high pressures and PC phases at high temperatures. Whether real water does indeed form PC phases or fcc solid structures is an issue that can be solved only by performing experimental work. Experimental studies proving or disproving the existence of a PC phase for water, should be of great interest not only for the people interested in high pressure studies of water but also for the broad research community performing computer simulations involving water.

II. SIMULATION DETAILS

We have performed Monte Carlo (MC) and molecular dynamics (MD) simulations for PC phases of water (bcc and fcc). We have used the TIP4P/2005,[37] TIP4P,[36] and SPC/E (Ref. 35) models. They are rigid and nonpolarizable models. A LJ center is located on the oxygen atom and positive charges are located on the hydrogen atoms. The negative charge is located on the H–O–H bisector for the TIP4P models and on the oxygen for the SPC/E model. In Ref. 38 one can find a critical comparison of the performance of these three popular water models.

The number of molecules used in the simulations were 432 for the bcc PC [which corresponds to 216 units cells $(6\times6\times6)$], 500 for the fcc PC [125 units cells $(5\times5\times5)$], 432 for ice VII [216 units cells $(6\times6\times6)$], and either 360 or 432 molecules for the fluid phase. In all cases the LJ potential was truncated at 8.5 Å. Standard long range corrections to the LJ part of the potential were added. The Ewald summation technique has been employed for the calculation of the long range Coulombic forces. We have performed isotropic and anisotropic NpT simulations. In the isotropic simulations the volume of the system fluctuates but the shape of the simulation box remains constant. In anisotropic NpT the volume and the shape of the simulation box are allowed to fluctuate.[49,50] For fluid water and for the cubic solids (ice VII and the two PCs) we used isotropic scaling. In one case anisotropic scaling was used for the bcc PC to analyze its possible transformation into a fcc PC through a Martensitic phase transition.[51] A typical MC run involves about 30 000 cycles of equilibration and 70 000 cycles to obtain averages (defining a cycle as a trial move per particle plus a trial volume move).

To determine the phase diagram free energy calculations are required. Free energy calculations can be determined with the Einstein crystal method[52–54] or a modified version denoted as the Einstein molecule approach.[55] The technique can be used for ices and details have been provided elsewhere.[56,57] By applying two external fields, one translational forcing the molecules to occupy a certain position, and another orientational forcing the molecules to adopt a certain

orientation we have been able to compute the free energy of a number of solid phases of water. However, the application of the technique to PCs may be problematic as at low values of the orientational field very long runs should be performed to guarantee that the molecules are able to rotate as in the PC. To avoid this issue we have developed a new method for free energy calculations of PCs, which allow us to avoid connecting orientational springs to the molecules. The difference with the traditional Einstein crystal as applied to other ices is that for the PCs only translational springs will be used. The method is inspired in the methodology proposed by Lindberg and Wang[58] to evaluate dielectric constants of ices.

An ideal Einstein crystal with the center of mass (CM) fixed is used as the reference system to compute the free energy. Let us describe the different steps to computing the free energy of a PC:

(1) An ideal Einstein crystal is a solid in which the molecules are bound to their lattice positions by harmonic springs. For PCs only translational (and not orientational) springs will be used (this prevents the appearance of phase transitions along the integration). The energy of the ideal Einstein crystal is given by

$$U_{\mathrm{Ein}} = \sum_{i=1}^{N} \Lambda_E (\mathbf{r_i} - \mathbf{r_{i0}})^2, \tag{1}$$

where $\mathbf{r}_i$ represents the instantaneous location of the reference point of molecule i and $\mathbf{r}_{i0}$ denotes its equilibrium position. U_{Ein} is a harmonic field that tends to keep the molecules at their lattice positions. Λ_E is the coupling parameter of the translational springs and has units of energy over a squared length. The free energy of the ideal Einstein crystal (with translational springs) with fixed CM ($A^{\mathrm{CM}}_{\mathrm{Ein\text{-}id}}$) is given by[53,56]

$$A^{\mathrm{CM}}_{\mathrm{Ein\text{-}id}} = -k_B T \ln Q^{\mathrm{CM}}_{\mathrm{Ein},t}, \tag{2}$$

$$= -k_B T \ln\left[P^{\mathrm{CM}} \left(\frac{\pi}{\beta \Lambda_E} \right)^{3(N-1)/2} (N)^{3/2} \right], \tag{3}$$

where $P^{\mathrm{CM}} = (1/\Lambda^{3(N-1)}) N^{-3/2}$ and Λ is the thermal De Broglie wavelength ($\Lambda = (h^2/2\pi m k_B T)^{1/2}$), which has units of length.

(2) To the ideal Einstein crystal described above we incorporate intermolecular interactions in the form of a LJ potential (whose parameters σ and ϵ are identical to those of the water model under consideration). The difference in free energy between the Einstein crystal with LJ interactions ($A^{\mathrm{CM}}_{\mathrm{Ein\text{-}LJ}}$) and the noninteracting Einstein crystal ($A^{\mathrm{CM}}_{\mathrm{Ein\text{-}id}}$) both with fixed CM can be obtained in a perturbative way as

$$\Delta A_1 = A^{\mathrm{CM}}_{\mathrm{Ein\text{-}LJ}} - A^{\mathrm{CM}}_{\mathrm{Ein\text{-}id}} = U_{\mathrm{lattice}} - k_B T \ln \langle \exp[-\beta (U_{\mathrm{sol}} - U_{\mathrm{lattice}})] \rangle_{\mathrm{Ein\text{-}id}}, \tag{4}$$

where U_{lattice} is the energy of the system when the molecules stand fixed on the lattice position (i.e., the LJ lattice energy) and U_{sol} is the LJ energy of the system for the considered configuration. The average is performed over configurations generated for the ideal Einstein crystal.

(3) Then we evaluate the free energy difference between an Einstein crystal with water interactions (i.e., TIP4P/2005, SPC/E, etc.) and an Einstein crystal with LJ interactions, both with fixed CM. To evaluate this free energy difference, the charges of the water potential are turned on, while keeping the translational springs. The path linking the LJ potential to the water potential is defined as

$$U(\lambda_Q) = (1 - \lambda_Q) U_{\mathrm{LJ}} + \lambda_Q U_{\mathrm{water}}, \tag{5}$$

$$\Delta A_Q = A^{\mathrm{CM}}_{\mathrm{Ein\text{-}sol}} - A^{\mathrm{CM}}_{\mathrm{Ein\text{-}LJ}} = \int_0^1 \langle U_{\mathrm{water}} - U_{\mathrm{LJ}} \rangle_{N,V,T,\lambda_Q} d\lambda_Q, \tag{6}$$

where $\langle U_{\mathrm{water}} - U_{\mathrm{LJ}} \rangle_{N,V,T,\lambda_Q}$ can be obtained in a NVT simulation at a given λ_Q. As the reference LJ potential has the same parameters as the LJ part of the water potential then $\langle U_{\mathrm{water}} - U_{\mathrm{LJ}} \rangle_{N,V,T,\lambda_Q}$ is simply the Coulombic contribution to the energy of the water potential U_Q and Eq. (2) can be rewritten as

$$\Delta A_Q = \int_0^1 \langle U_Q \rangle_{N,V,T,\lambda_Q} d\lambda_Q. \tag{7}$$

Since we are not using orientational springs the molecules are able to rotate at the beginning (when $\lambda_Q = 0$) and at the end (when $\lambda_Q = 1$) of the integration avoiding the possible existence of a phase transition along the integration path. The value of the integral is then obtained numerically.

(4) Now the translational springs are turned off gradually. The free energy change ΔA_2 between the water molecules bonded to their lattice positions by harmonic springs ($A^{\mathrm{CM}}_{\mathrm{Ein\text{-}sol}}$) and the PC with no translational springs (both with fixed CM) is given by

$$\Delta A_2 = A^{\mathrm{CM}}_{\mathrm{sol}} - A^{\mathrm{CM}}_{\mathrm{Ein\text{-}sol}} = -\int_0^{\Lambda_E} \frac{\langle U_{\mathrm{Ein\text{-}id}} \rangle_{N,V,T,\lambda}}{\Lambda_E} d(\lambda \Lambda_E). \tag{8}$$

Since the integrand changes by several orders of magnitude it is convenient to perform a change in variable[52,59] from $\lambda\Lambda_E$ to $\ln(\lambda\Lambda_E + c)$, where c is a constant. We shall use $c = \exp(3.5)$ which significantly smoothes the integrand. The final expression for ΔA_2 is

$$\Delta A_2 = -\int_{\ln(c)}^{\ln(\Lambda_E + c)} \frac{\langle U_{\mathrm{Ein\text{-}id}} \rangle_{N,V,T,\lambda} (\lambda \Lambda_E + c)}{\Lambda_E} \times d(\ln(\lambda \Lambda_E + c)). \tag{9}$$

Fixing the CM avoids the quasidivergence of the integrand of Eq. (9) when the coupling parameter λ tends to zero. Without this constraint, the integrand would increase sharply in this limit, making the evaluation of the integral numerically involved.

(5) The last step is to evaluate the free energy change between a PC with no constraint and the PC with a fixed CM. The free energy change in this last step ΔA_3 is given by

$$\Delta A_3 = A_{\mathrm{sol}} - A_{\mathrm{sol}}^{\mathrm{CM}} = -k_B T \ln \frac{Q_{\mathrm{sol}}}{Q_{\mathrm{sol}}^{\mathrm{CM}}} = k_B T[\ln(P^{\mathrm{CM}}/P) - \ln(V/N)], \tag{10}$$

where $P=1/\Lambda^{3N}$. ΔA_3 does not depend on the particular form of the intermolecular potential U_{sol}.

The final expression of the free energy of the PC is

$$A_{\mathrm{sol}} = (A_{\mathrm{Ein\text{-}id}}^{\mathrm{CM}} + \Delta A_3) + \Delta A_1 + \Delta A_Q + \Delta A_2 = A_0 + \Delta A_1 + \Delta A_Q + \Delta A_2. \tag{11}$$

Placing together the $A_{\mathrm{Ein\text{-}id}}^{\mathrm{CM}}$ and ΔA_3 terms (A_0), the P^{CM} contribution cancels out and the final expression of the free energy of the PC solid is

$$\frac{A_{\mathrm{sol}}}{Nk_BT} = -\frac{1}{N}\ln\left[\left(\frac{1}{\Lambda}\right)^{3N}\left(\frac{\pi}{\beta\Lambda_E}\right)^{3(N-1)/2}(N)^{3/2}\frac{V}{N}\right] + \left[\frac{U_{\mathrm{lattice}}}{Nk_BT} - \frac{1}{N}\ln\langle\exp[-\beta(U_{\mathrm{sol}}-U_{\mathrm{lattice}})]\rangle_{\mathrm{Ein\text{-}id}}\right] + \int_0^1 \left\langle \frac{U_Q}{Nk_BT}\right\rangle_{N,V,T,\lambda_Q} d\lambda_Q - \int_0^1 \left\langle \frac{U_{\mathrm{Ein\text{-}id}}}{Nk_BT}\right\rangle_{N,V,T,\lambda} d\lambda. \tag{12}$$

The first term corresponds to A_0, the second to ΔA_1, the third to ΔA_Q, and the last term to ΔA_2.

The free energy was computed at a certain thermodynamic state. By using thermodynamic integration the free energy for other thermodynamic conditions can be obtained easily. The free energy of the fluid phase was obtained as described in our previous work.[56] The chemical potential is easily obtained as $\mu/k_BT=G/Nk_BT=(A/Nk_BT)+(pV/Nk_BT)$. Once the free energies (and chemical potentials) for the fluid and for the different solid phases are known initial coexistence points can be located by imposing the condition of equal chemical potential $(\mu_{\mathrm{I}}=\mu_{\mathrm{II}})$ at the same temperature and pressure. Having an initial coexistence point the rest of the coexistence curve can be obtained by using Gibbs–Duhem integration.[60,61] This technique allows one to determine the coexistence line between two phases, provided that an initial coexistence point is known. Gibbs–Duhem is a numerical integration of the Clapeyron equation (and where volume and enthalpy changes are obtained by using computer simulations). The Clapeyron equation is given by

$$\frac{dp}{dT} = \frac{s_{\mathrm{II}} - s_{\mathrm{I}}}{v_{\mathrm{II}} - v_{\mathrm{I}}} = \frac{h_{\mathrm{II}} - h_{\mathrm{I}}}{T(v_{\mathrm{II}} - v_{\mathrm{I}})}. \tag{13}$$

Subscripts I and II label the corresponding phases and the thermodynamic properties written with small letters are properties per particle $(x=X/N)$. For the integration of the Clapeyron equation a fourth-order Runge–Kutta integration is employed.

In this work free energy calculations were performed only for the TIP4P/2005 model. To obtain initial coexistence points for the TIP4P and SPC/E models of water we shall use Hamiltonian Gibbs–Duhem integration. Hamiltonian Gibbs–Duhem integration is a very powerful technique that allows one to determine the change in the coexistence conditions of a certain coexistence line due to a change in the water potential. In this kind of integration the Hamiltonian of the system is changed through a coupling parameter (so that $\lambda=0$ for the initial Hamiltonian and $\lambda=1$ for the final Hamiltonian). When the coupling parameter (λ) is introduced within the expression of the potential energy of the system $(U(\lambda))$, then a set of generalized Clapeyron equations can be derived. The derivation is as follows. For two phases at coexistence,

$$g_{\mathrm{I}}(T,p,\lambda) = g_{\mathrm{II}}(T,p,\lambda). \tag{14}$$

If the system is perturbed slightly while preserving the coexistence it must hold that

$$-s_{\mathrm{I}}dT + v_{\mathrm{I}}dp + \left(\frac{\partial g_{\mathrm{I}}}{\partial\lambda}\right)d\lambda = -s_{\mathrm{II}}dT + v_{\mathrm{II}}dp + \left(\frac{\partial g_{\mathrm{II}}}{\partial\lambda}\right)d\lambda. \tag{15}$$

If the coupling parameter remains constant when performing the perturbation then one recovers the traditional Clapeyron Eq. (13)(coexistence on the p-T plane). If the pressure is kept constant when the perturbation is performed (coexistence on the λ-T plane) then one obtains

$$\frac{dT}{d\lambda} = \frac{T\left[\frac{\partial g_{\mathrm{II}}}{\partial\lambda} - \frac{\partial g_{\mathrm{I}}}{\partial\lambda}\right]}{h_{\mathrm{II}} - h_{\mathrm{I}}}. \tag{16}$$

The property $\partial g/\partial\lambda=\langle\partial u(\lambda)/\partial\lambda\rangle_{N,p,T,\lambda}$, can be determined easily during the NpT simulations. Then Eq. (16) can be rewritten as

$$\frac{dT}{d\lambda} = \frac{T\left[\left\langle\left(\frac{\partial u_{\mathrm{II}}(\lambda)}{\partial\lambda}\right)\right\rangle - \left\langle\left(\frac{\partial u_{\mathrm{I}}(\lambda)}{\partial\lambda}\right)\right\rangle\right]}{h_{\mathrm{II}} - h_{\mathrm{I}}}. \tag{17}$$

This generalized Clapeyron Eq. (16) can be integrated numerically (from $\lambda=0$ to $\lambda=1$) to obtain the coexistence temperature (at a certain fixed pressure) of the water potential of interest, provided that the coexistence temperature is known for the initial reference potential.

A similar equation can be obtained when a perturbation is performed (while keeping the temperature constant). In this case the coexistence pressure of the water potential of interest is obtained (at a certain fixed temperature) provided that the initial coexistence pressure is known for the initial reference potential. The working expression is

$$\frac{dp}{d\lambda} = -\frac{\left\langle\left(\frac{\partial u_{\mathrm{II}}(\lambda)}{\partial\lambda}\right)\right\rangle - \left\langle\left(\frac{\partial u_{\mathrm{I}}(\lambda)}{\partial\lambda}\right)\right\rangle}{v_{\mathrm{II}} - v_{\mathrm{I}}}. \tag{18}$$

Let us assume that λ is as a coupling parameter leading the system from a certain reference potential U_A to the potential of interest U_B. This can be done with a coupling of the form,

$$U(\lambda) = \lambda U_B + (1-\lambda)U_A, \tag{19}$$

with λ changing from zero (initial reference potential) to one (final potential of interest). The generalized Clapeyron equations can be written as

$$\frac{dT}{d\lambda} = \frac{T(\langle u_B - u_A\rangle^{\mathrm{II}}_{N,p,T,\lambda} - \langle u_B - u_A\rangle^{\mathrm{I}}_{N,p,T,\lambda})}{h_{\mathrm{II}} - h_{\mathrm{I}}}, \tag{20}$$

$$\frac{dp}{d\lambda} = -\frac{\langle u_B - u_A\rangle^{\mathrm{II}}_{N,p,T,\lambda} - \langle u_B - u_A\rangle^{\mathrm{I}}_{N,p,T,\lambda}}{v_{\mathrm{II}} - v_{\mathrm{I}}}, \tag{21}$$

where u_B is the internal energy per molecule when the interactions between molecules are described by U_B (and analogous definition is used for u_A). If a coexistence point between two phases is known for potential A then integration of the previous equations from $\lambda=0$ to $\lambda=1$ allows one to determine the coexistence point between these two phases for potential B. This can be done either by fixing the temperature or the pressure along the integration.

To estimate nucleation times of the PC phases and to determine the melting point of the fcc PC phase by direct coexistence technique we have performed MD simulations using the program GROMACS.[62] In these simulations the temperature is kept constant by using a Nose–Hoover thermostat[63,64] with a relaxation time of 2 ps. To keep the pressure constant, a Parrinello–Rahman barostat[49,51] (isotropic or anisotropic) was used. The relaxation time of the barostat was 2 ps. The time step was 1 fs and the typical length of the runs was of about 5 ns. The geometry of the water molecules is enforced using constraints. The LJ part of the potential was truncated at 8.5 Å and standard long range correction were added. Ewald sums are used to deal with the long range Coulombic interactions. Coulombic interactions in real space were truncated at 8.5 Å. The Fourier part of the Ewald sums was evaluated using the particle mesh Ewald.[65] The width of the mesh was 1 Å and we used a fourth order interpolation.

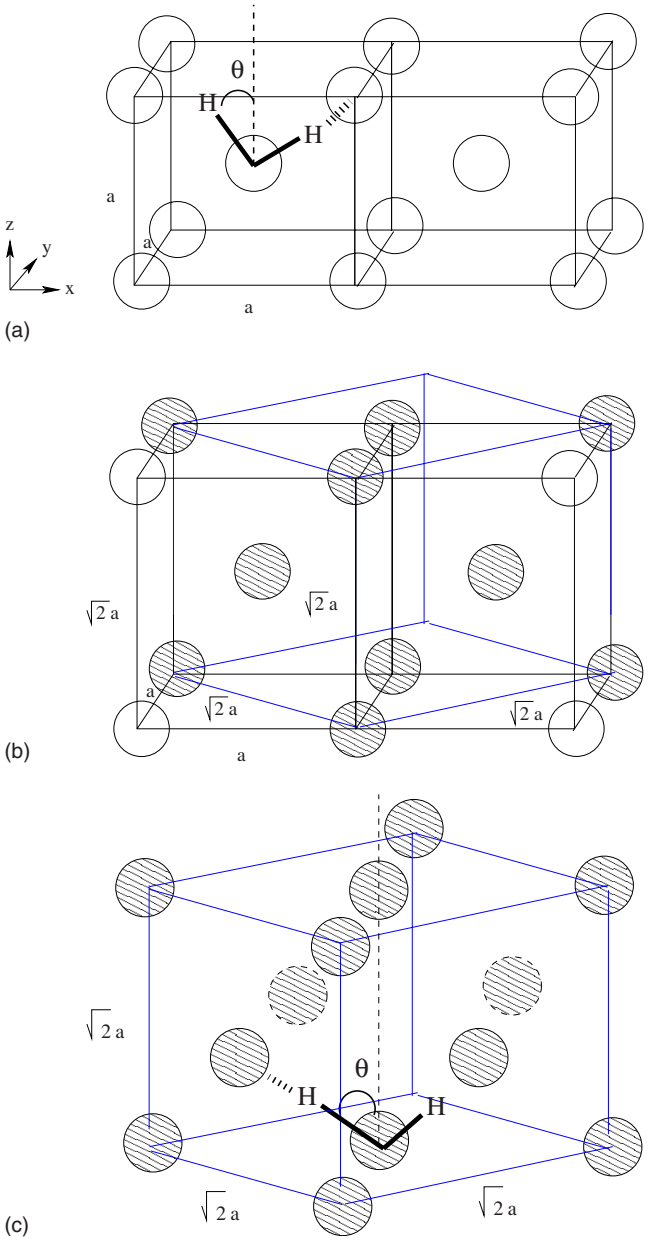

FIG. 2. (Color online) (a) Two bcc unit cells. (b) How the fcc lattice can be obtained from two bcc cells. When the z direction is scaled by $\sqrt{2}a$, the crystal is transformed into a fcc lattice. (c) fcc unit cell.

III. RESULTS

For the TIP4P/2005 model we found in previous work that ice VII transformed into a bcc PC at 377 K when heated along 70 000 bars isobar.[40] We shall now explore the stability of this bcc PC. It is well known that a bcc solid can transform into a fcc solid, provided that the fcc is more stable, and that one uses anisotropic NpT simulations (Rahman–Parrinello NpT). We shall explore the behavior of the bcc PC solid when heated along the 70 000 bars isobar. The bcc PC is stable when heating up to temperatures of about 460 K (even though we are using anisotropic NpT simulations and it could transform into a fcc solid) but at 480 K the properties of the system (energies, densities, and shape of the simulation box) undergo a clear jump. A Martensitic phase transition occurs in which the bcc lattice is transformed into a fcc lattice by increasing the c edge of the bcc structure. The simulation box that was originally cubic for the bcc PC becomes tetragonal (a sketch of the transformation is given in Fig. 2). In Fig. 3 the instantaneous values of the lengths of the sides of the simulation box are presented for a temperature of 440 K and for a temperature of 480 K. As can be seen at 440 K one sees fluctuations of three sides of identical (in average) lengths. However, for the run performed at 480 K one of the sides increases slightly its length at the beginning of the run and after 40 000 cycles increases its length dramatically. At the end of the 480 K run the length of the sides are $a=17.608$: $b=17.620$; $c=25.557$. As can be seen the ratio c/a is close to $c/a=\sqrt{2}\simeq 1.414$, which is the value expected for the ratios of c and a in a Martensitic transformation from a bcc to a fcc solid (see the sketch of Fig. 2). Therefore, the ratio c/a (actually the ratio between the longest and the shortest sides of the simulation box since the Martensitic

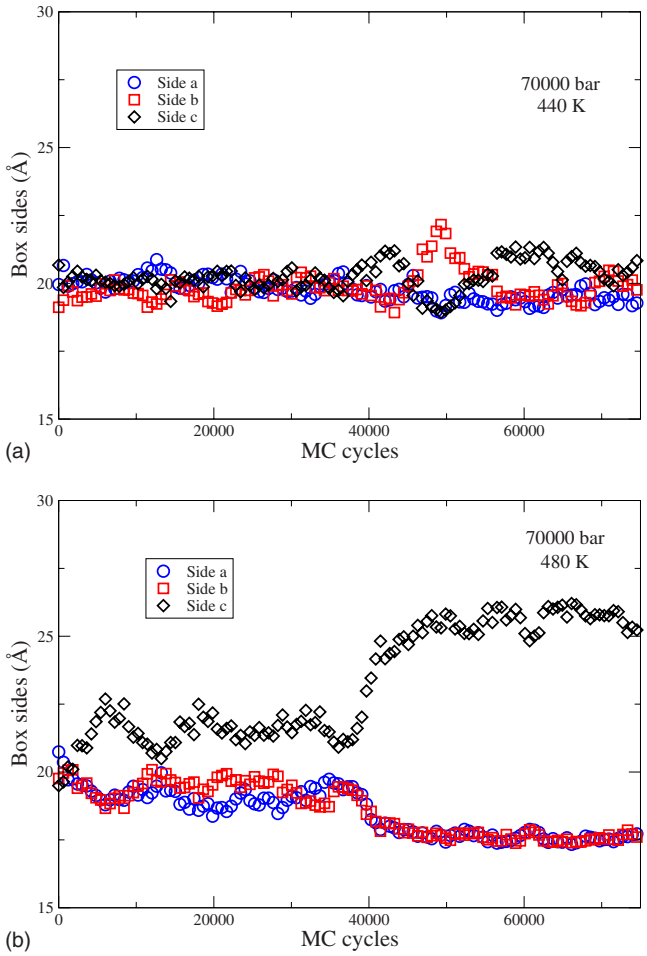

FIG. 3. (Color online) Simulation box sides change along the MC run (anisotropic NpT ensemble) for the bcc PC phase. (a) 440 K and 70 000 bars. (b) 480 K and 70 000 bars.

transition may occur also along the x or y axis) is a good order parameter to detect the transformation. In Fig. 4 the c/a ratio is plotted as a function of temperature for runs performed along the 60 000, 70 000, and 80 000 bars isobars. For the pressure 60 000 bars no bcc to fcc transition is observed. For the runs at 70 000 bars the transition occurs at

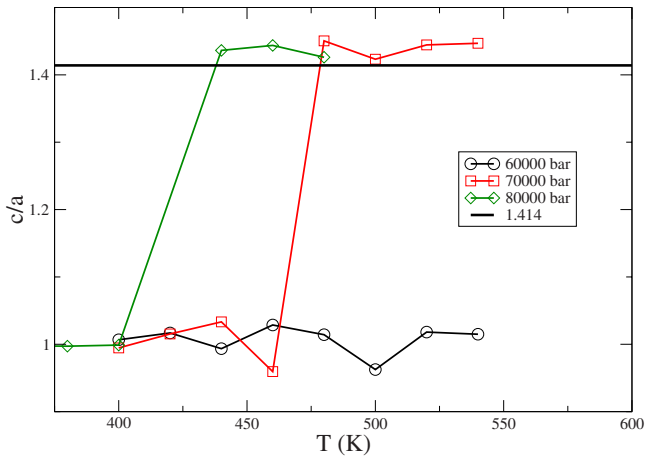

FIG. 4. (Color online) Temperature dependence of the c/a ratio at different pressures, 60 000 bars (open circles), 70 000 bars (open squares), and 80 000 bars (open diamonds).

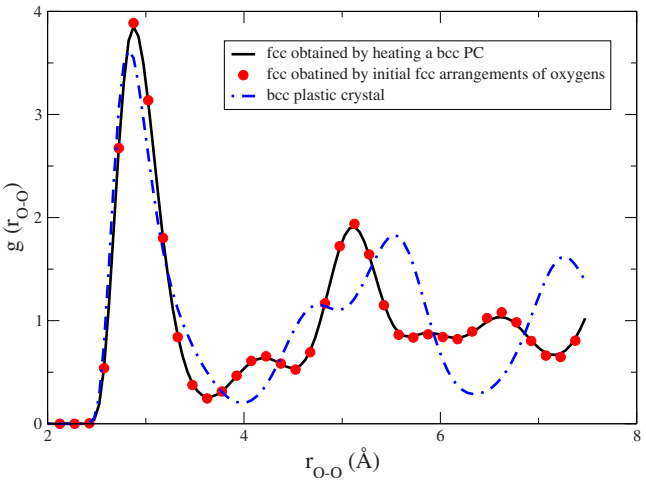

FIG. 5. (Color online) Oxygen-oxygen radial distribution functions at $T=440$ K and $p=80\,000$ bars for the fcc PC phase and at $T=440$ K and $p=70\,000$ bars for the bcc PC. fcc PC obtained by heating the bcc PC (solid line), fcc PC obtained by the fcc lattice of the oxygens (filled circles), and bcc PC (dashed-dotted line). Notice that the correct g_{O-O} and g_{O-H} in Figs. 2, 4, and 5 of our previous work (Ref. 40) are obtained by shifting the curves 0.5 Å to the right.

about 480 K. For the runs at 80 000 bars the transition occurs at about 420 K. Therefore the transition temperature decreases as the pressure increases. That suggests a negative slope of the bcc-fcc coexistence line. Notice that the jump in Fig. 4 does not correspond to the true coexistence point (i.e., identical chemical potential) between these two phases. Packing considerations favor the fcc structure with respect to the bcc structure. In fact for a r^{-12} potential Wilding[66] found recently that the fcc structure is more stable than the bcc.

We have found that the fcc PC could also be generated easily by starting from a fcc arrangement of the oxygen atoms (and introducing random orientations). In fact we generated the fcc PC starting from a fcc solid of 500 molecules (i.e., 125 unit cells). In Fig. 5 the oxygen-oxygen radial distribution function (g_{O-O}) is shown. As can be seen the radial distribution function of the solid obtained from the Martensitic transformation is identical to that obtained from an initial fcc arrangement of oxygens. The radial distribution function of the fcc PC is clearly different from that of the bcc PC. In fact the bcc PC shows the first peak of the g_{O-O} at 2.81 Å, the second at 4.59 Å, and the third at 5.50 Å, whereas fcc PC has a first peak at 2.87 Å and the second and third peaks move apart and shift to shorter distances, 4.16 and 5.10 Å, respectively (Fig. 5).

We have computed the powder x-ray and neutron diffraction patterns. The intensity of the diffraction peaks is obtained as

$$\mathrm{I} = \frac{P(\theta)}{\mathrm{sen}(\theta)\mathrm{sen}(2\theta)} m_i |F_{hkl}|^2, \tag{22}$$

where m_i is the multiplicity and $P(\theta)$ is the polarization factor [in neutron diffraction $P(\theta)=1$ and in x-ray diffraction $P(\theta)=(1+\cos^2(2\theta)/2)$]. In the x-ray diffraction pattern, the F_{hkl} is obtained as

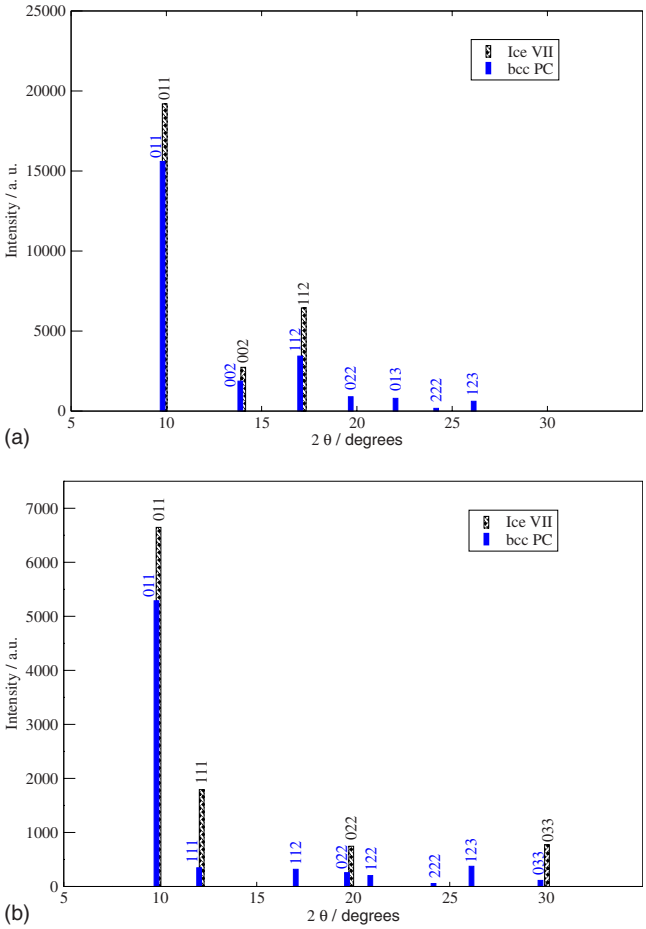

FIG. 6. (Color online) (a) Simulated powder x-ray diffraction pattern for ice VII (dashed line) at 70 000 bars and 300 K and bcc PC (solid line) at 70 000 bars and 400 K. The wavelength used was 0.4 Å. The Miller indices *hkl* are given for each peak. (b) Simulated neutron diffraction pattern for ice VII (dashed line) at 70 000 bars and 300 K and bcc PC (solid line) at 70 000 bars and 400 K. The wavelength was 0.4 Å. The Miller indices *hkl* are given for each peak.

$$F_{hkl} = \frac{1}{N}\sum_{n=1}^{N} f_n(\theta) e^{2\pi i(hx_n + ky_n + lz_n)}, \tag{23}$$

where $f_n(\theta)$ is function of θ. Both oxygen and hydrogens were considered and $f_n(\theta)$ was obtained from the fit proposed by Lee and Pakes.[67] The wavelength (λ) used was 0.4 Å.[11,13] In the neutron diffraction pattern (which was calculated for heavy water) F_{hkl} was obtained as

$$F_{hkl} = \frac{1}{N}\sum_{n=1}^{N} b_n e^{2\pi i(hx_n + ky_n + lz_n)}, \tag{24}$$

where the neutron scattering amplitudes (b_n) of the deuteron and the oxygen atom are 0.6671 and 0.5803 fm, respectively, and do not depend on θ.[68] The wavelength used was also 0.4 Å. The number of molecules used in these simulations were 1024 (512 unit cells) and we checked that the bcc PC also appears for this system size. Results are presented in Fig. 6. The main difference between the ice VII and bcc PC x-ray diffraction patterns is the intensity reduction, around 20%, for the bcc PC peaks and the appearance of more peaks at large 2θ values for the bcc PC. The same results are observed on the neutron diffraction pattern [Fig. 6(b)]. The intensity reduction of the diffraction peaks is not surprising if one takes into account that in ice VII the hydrogen bonds maintain the location of the oxygen atoms more or less fixed (except for some slight thermal vibration). However in the PC phases the molecules are free to rotate (frequently forming and breaking hydrogen bonds) so the oxygen atom is able to move significantly from its equilibrium lattice position. The bcc PC diffraction peaks were shifted to lower 2θ values with respect to ice VII due to the lower density of this phase. The conclusion of these results is that one of the signatures of the formation of a PC phase (say the bcc) will be a significant reduction in the intensity of the diffraction lines with respect to ice VII. Observing the intensity ratio between the 011 and 111 peaks (I_{011}/I_{111}) on the neutron diffraction pattern for ice VII and bcc PC, we can see that its value is of about 4 for ice VII and of about 15 for bcc PC. Therefore the ratio I_{011}/I_{111} could be used to detect the appearance of the bcc PC.

To gain further understanding of the orientational order in the PC phases we have also determined the probability distribution of the polar angles (θ and ϕ of the OH bonds). The x axis is located on the **a** vector of the unit cell, the y axis is located on the **b** vector of the unit cell, and the z axis is located along the **c** vector of the unit cell [see Figs. 2(a) and 2(c)]. The distribution function $f(\theta)$ is defined as

$$f(\theta) = \frac{N(\theta)}{2N\Delta\theta}, \tag{25}$$

where $N(\theta)$ denotes the number of OH bonds with polar angle between θ and $\theta+\Delta\theta$ and $2N$ is the number of OH bonds (i.e., twice the number of molecules N). The distribution function $f(\phi)$ is defined as

$$f(\phi) = \frac{N(\phi)}{2N\Delta\phi}. \tag{26}$$

In Fig. 7 the functions $f(\theta)$ and $f(\phi)$ are presented for ice VII at 300 K and 70 000 bars, bcc PC at 400 K and 70 000 bars and fcc PC at 440 K and 80 000 bars. For the PC phases, bcc and fcc, the distribution functions $f(\theta)$ and $f(\phi)$ are more uniform than those of ice VII. This is due to the fact that in the PC phases the molecules are able to rotate almost freely. Nevertheless the angular distribution is not uniform even in the PC phase since the OH vectors still prefer to point out to the contiguous oxygen atoms. For bcc PC and ice VII the peaks of $f(\theta)$ are located at 54.74 and (180 −54.74) where 54.74 is the angle between one of the diagonals of the cube and a line connecting the center of two opposite faces [Fig. 2(a)]. However, for the fcc PC the peaks of $f(\theta)$ are located at 45°, 90°, and 135°. Where 45 and 135 are the angles between one of the diagonals that is connecting the center of two perpendicular faces of the cube and the z edge [Fig. 2(c)] and 90 is the angle between the line connecting two oxygens resting on the same plane with the z edge. For the bcc PC the angles 0°, 90°, and 180° in the $f(\theta)$ have nonzero probability. This provides some indication that in the bcc PC the OH vectors point sometimes (while rotating) to second nearest neighbors. For ice VII and the bcc PC,

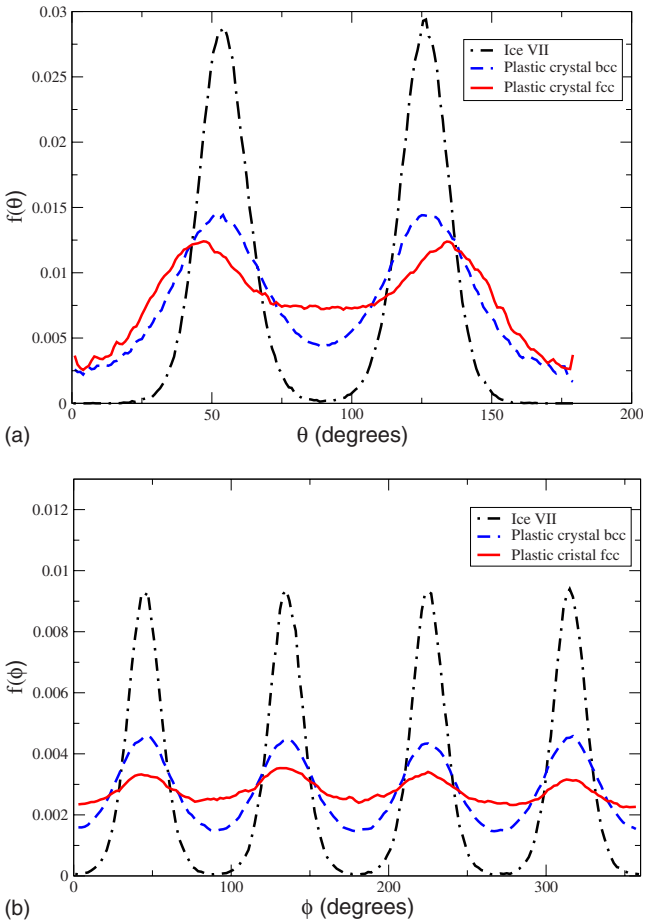

FIG. 7. (Color online) (a) $f(\theta)$ as a function of θ angle for ice VII (dashed-dotted line) at 300 K and 70 000 bars, for the bcc PC (dashed line) at 400 K and 70 000 bars and for the fcc PC (solid line) at 440 K and 80 000 bars. (b) $f(\phi)$ as a function of ϕ angle for the ice VII (dashed-dotted line) at 300 K and 70 000 bars, for the bcc PC (dashed line) at 400 K and 70 000 bars and for the fcc PC (solid line) at 440 K and 80 000 bars.

the angular distribution $f(\phi)$ presents four peaks separated by 90° as should be the case. In the fcc PC the function $f(\phi)$ is almost uniform, indicating that the molecules can rotate quite freely. For ice VII at 300 K and 70 000 bars and for the length of the simulations performed in this work, a certain individual molecule presents a fixed value of θ and ϕ (subject to some thermal vibration). However for the PC phases each individual molecule jumps quite often from one of the peaks of the distribution to another peak. These flipping or jumping moves occur quite often for each molecule within the length of the simulation runs considered here. Another way to see this orientational disorder is by means of the visualization of the MD trajectories. Multimedia mpg files for the MD trajectories of ice VII, bcc PC, and fcc PC are provided as electronic supplementary information.[69]

Let us now determine coexistence points between the different solid phases considered in this work (fluid, ice VII, bcc PC, and fcc PC). This requires free energy calculations for the different phases involved. Free energies for the liquid and for ice VII were obtained in our previous work.[40] We have determined the Helmholtz free energy for the bcc PC and fcc PC at 440 K and for the densities which correspond to that of the systems at 80 000 bars. The free energies are presented in Table I. For the fcc solid we have computed the free energy for a cubic simulation box (500 molecules) and for the tetragonal simulation box obtained from the Martensitic transition of the bcc PC (432 molecules). As can be seen the free energy of these two systems is the same. The small difference may be attributed to the different orientations of the crystallographic planes with respect to the periodic boundary conditions.[70] For the studied thermodynamic state (80 000 bars and 440 K), the fcc PC is more stable than bcc

TABLE I. Helmholtz free energy for ice VII, bcc PC phase, and fcc PC phase (as obtained with the Einstein crystal methodology). The Gibbs free energy was computed after adding pV to the Helmholtz free energy. The density is given in g/cm^3. The cubic fcc* phase correspond to the fcc PC phase obtained by heating the bcc PC phase.

Phase	Molecules	T (K)	P (bar)	ρ	A/Nk_BT	G/Nk_BT
Ice VII	432	300	70 000	1.707	−9.75	19.87
Cubic bcc	432	440	80 000	1.662	−3.93	19.78
Cubic fcc	500	440	80 000	1.679	−4.86	19.23
Cubic fcc*	432	440	80 000	1.679	−4.89	19.21
Cubic fcc	500	440	105 000	1.749	−3.76	25.80

TABLE II. Melting curves of the PC phases of the TIP4P/2005 as obtained from free energy calculations and Gibbs–Duhem integration (with isotropic NpT simulation performed for the fluid and for the PC phases). The densities are given in g/cm^3. The residual internal energies are given in kcal/mol. The * indicate the initial coexistence point.

T (K)	p (bar)	U_1	U_2	ρ_1	ρ_2
		Fluid-bcc PC			
340.00	60 193	−10.45	−10.03	1.574	1.622
* 400.00	62 000	−9.87	−9.58	1.562	1.609
440.00	64 390	−9.52	−9.30	1.564	1.608
460.00	66 042	−9.35	−9.12	1.560	1.607
520.00	71 653	−8.86	−8.71	1.563	1.615
		↓ Metastable			
600.00	80 608	−8.20	−8.13	1.575	1.626
700.00	93 249	−7.38	−7.37	1.599	1.646
900.00	121 380	−5.77	−5.92	1.636	1.690
1000.00	137 036	−4.96	−5.15	1.657	1.713
		Fluid-fcc PC			
* 440.00	66 790	−9.52	−9.06	1.575	1.628
500.00	70 691	−9.00	−8.67	1.566	1.629
520.00	72 435	−8.86	−8.54	1.569	1.629
540.00	74 164	−8.68	−8.44	1.575	1.633
560.00	76 115	−8.56	−8.29	1.569	1.635
		↑ Metastable			
600.00	80 089	−8.21	−8.03	1.571	1.639
650.00	85 533	−7.83	−7.71	1.581	1.648
700.00	91 508	−7.44	−7.37	1.590	1.657
720.00	93 955	−7.30	−7.21	1.593	1.661
740.00	96 444	−7.14	−7.09	1.597	1.663
760.00	98 973	−6.96	−6.97	1.599	1.667
780.00	101 586	−6.81	−6.80	1.602	1.672
800.00	104 216	−6.66	−6.67	1.607	1.677
900.00	118 027	−5.85	−5.99	1.625	1.698
1000.00	132 701	−5.10	−5.28	1.649	1.719

TABLE III. Solid-solid coexistence lines of the TIP4P/2005 model for the high pressure polymorphs (ice VII, PC bcc and PC fcc) as obtained from free energy calculations and Gibbs–Duhem integration. The densities are given in g/cm^3. The internal energies in kcal/mol (only the residual part of the internal energy is reported). The * indicate the initial coexistence point.

T (K)	p (bar)	U_1	U_2	ρ_1	ρ_2
		VII-bcc PC			
600.00	250 304	−4.13	−3.54	1.979	1.972
550.00	190 835	−6.11	−5.50	1.902	1.889
500.00	143 221	−7.67	−7.04	1.828	1.810
440.00	101 354	−8.99	−8.49	1.749	1.728
400.00	80 146	−9.76	−9.19	1.707	1.674
		↑ Metastable			
* 377.00	70 000	−10.04	−9.53	1.681	1.645
360.00	63 292	−10.27	−9.79	1.666	1.623
350.00	59 665	−10.40	−9.95	1.656	1.617
		VII-fcc PC			
* 393.00	77 179	−9.94	−9.04	1.703	1.677
414.75	100 000	−9.17	−8.34	1.752	1.740
446.94	200 000	−6.73	−5.43	1.938	1.935
441.29	400 000	−1.19	0.41	2.162	2.168
422.43	500 000	1.61	3.29	2.244	2.251
400.00	592 309	4.18	5.87	2.309	2.319
300.00	880 106	12.12	13.76	2.474	2.489
250.00	980 523	14.81	16.41	2.523	2.539
		bcc PC-fcc PC			
* 570.00	77 124	−8.35	−8.22	1.621	1.635
520.00	74 646	−8.65	−8.51	1.625	1.639
500.00	74 495	−8.75	−8.61	1.630	1.643
460.00	74 746	−8.97	−8.78	1.640	1.655
440.00	75 551	−9.03	−8.85	1.648	1.661
400.00	78 266	−9.20	−8.98	1.666	1.679
380.00	80 876	−9.44	−9.02	1.691	1.692

PC (it has a lower chemical potential). This is consistent with the results presented in Fig. 4 where it was shown that when anisotropic NpT simulations were used the bcc PC transformed into a fcc PC. Notice however that it is possible to have a mechanically stable bcc PC at 80 000 bars and 440 K provided that isotropic NpT simulations are performed (with this type of scaling the bcc PC remains mechanically stable) so it is possible to compute thermodynamic properties even under conditions where the solid is metastable from a thermodynamic point of view. In Table I the free energy is presented for two different thermodynamic states of the fcc PC. By using thermodynamic integration it is possible to estimate the free energy at 440 K and 105 000 bars starting from the value at 440 K and 80 000 bars. We obtain $-3.77Nk_BT$ which is good agreement with the value $-3.76Nk_BT$ obtained from Einstein crystal calculation (Table I).

By using thermodynamic integration the coexistence point between the fluid and the fcc PC has been located at 440 K and 66 790 bars. Once an initial coexistence point has been found for the fluid-fcc PC transition, the rest of the coexistence line will be obtained by Gibbs–Duhem integration. The fluid-bcc PC was integrated from the coexistence point given in our previous work at 400 K and 62 000 bars,

TABLE IV. New triple points for the TIP4P/2005, TIP4P, and SPC/E models. The rest of the triple points of the models were given in Refs. 40 and 71.

	TIP4P/2005		TIP4P		SPC/E	
Phases	T (K)	p (bar)	T (K)	p (bar)	T (K)	p (bar)
L-VII-bcc	352	60 375	322	58 929	347	71 284
L-bcc-fcc	570	77 124	520	73 100	683	103 426
VII-bcc-fcc	393	77 179	363	76 091	434	112 204

obtained by free energy calculations. The fluid-bcc PC and fluid-fcc PC coexistence lines meet at a triple point located around 570 K and 77 124 bars. This triple point can be used as initial coexistence point of the bcc PC-fcc PC coexistence curve. This curve intersects the ice VII-bcc PC coexistence line, generating a new triple point at 393 K and 77 179 bars. This triple point was used as initial point for the ice VII-fcc PC coexistence line. The new coexistence lines for the TIP4P/2005 model are given in tabular form in Tables II and III. The triple points generated by these coexistence lines are shown in Table IV. The rest of the triple points of these models can be found in Refs. 40 and 71.

Free energy calculation is somewhat involved and it is convenient to determine coexistence points by an independent procedure. For this reason we also used direct coexistence simulations to determine the fluid-fcc PC transition. The direct coexistence technique, was pioneered by Woodcok and co-workers.[72–74] An equilibrated configuration of a fcc PC phase (500 molecules) was located on the left hand side of the simulation box and put into contact with an equilibrated configuration of the fluid having 500 molecules. We then performed MD simulations using GROMACS, while keeping the temperature at 600 K. We performed several runs at different pressures. In Fig. 8, the evolution of the density with time is shown for several pressures. As we can see, for low pressures (70 000 and 79 000 bars) the density decreases indicating the melting of the fcc PC. For high pressures (80 500 and 90 000 bars) the density of the system

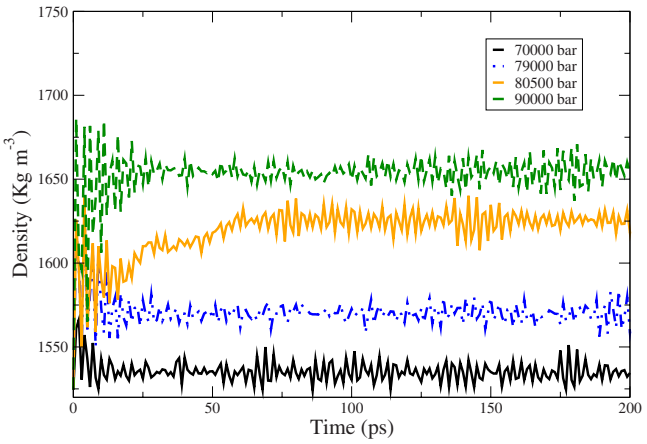

FIG. 8. (Color online) Evolution of the density with the time as obtained from direct coexistence MD simulations. All results were obtained for T =600 K. Lines from the top to the bottom correspond to the pressures 90 000, 80 500, 79 000, and 70 000 bars, respectively. For the two first pressures the liquid water freezes, whereas for the last two pressures the solid melts. The estimate coexistence pressure at 600 K is 79 750 bars.

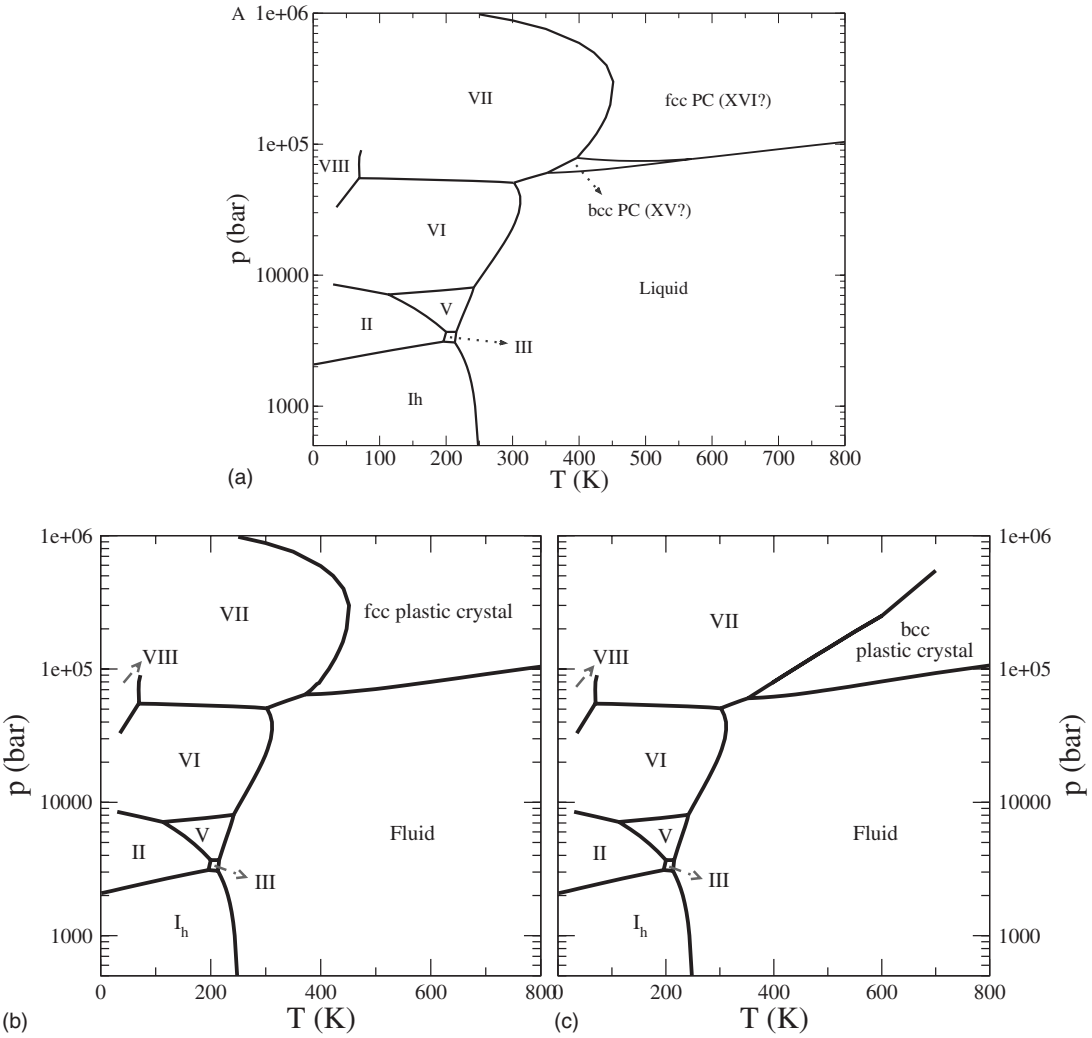

FIG. 9. (a) Global phase diagram for the TIP4P/2005 model. (b) What the phase diagram for the TIP4P/2005 model would be like if the bcc PC phase would be excluded. (c) What the phase diagram for the TIP4P/2005 model would be like if the fcc PC phase would be excluded.

increases indicating the freezing of the fluid into a fcc PC. This gives a coexistence pressure of about 79 750 bars. Thus, the value of about 80 000 obtained from free energy calculations is consistent with the results obtained from direct coexistence.

Dolan *et al.*,[39,75] showed that the formation of a high pressure ice phase from liquid water occurs in a few nanoseconds when the temperature is around 400 K. By using computer simulations we obtain further evidence of this by nucleating the bcc PC solid from the fluid in a few nanoseconds.[40] This nucleation time is small compared to that found previously for ice Ih (Ref. 41) (hundreds of nanoseconds). We will attempt here to nucleate the fcc PC solid. We performed MD simulations of the fluid phase with isotropic scaling using 500 molecules in a cubic simulation box [500 molecules is the number of water molecules required to form 125 unit cells of the fcc PC $4\times(5\times5\times5)$]. The simulations were performed at 600 K and 100 000 bars where the fcc PC is the thermodynamically stable phases. No nucleation of the fcc PC was observed after 12 ns. We then changed strategy and performed, with the same conditions, MD simulations with isotropic scaling of the sides of the simulation box, using a cubic box, containing 432 molecules. This number of molecules (432) corresponds to 216 unit cells of a bcc PC $(2\times(6\times6\times6))$. In this case we observed in most of the cases the formation of a bcc PC in a few nanoseconds (in fact the oxygen-oxygen radial distribution function was clearly that of the bcc PC). With this bcc PC nucleated from the fluid we then performed anisotropic *NpT* MD simulations. In most of the cases nothing happened, but in one of the runs the bcc PC transformed into a fcc PC through a Martensitic transformation. This typically occurred when the bcc PC obtained was free of defects and with their crystallographic axis aligned with the vectors of the simulation box. The overall picture is that the formation of the fcc PC from the fluid occurs in two steps. First, the bcc PC is formed. Then the bcc PC is transformed into the fcc PC via a Martensitic transition. This two step process is the most likely path to the nucleation of the fcc PC. It seems clear that the free energy nucleation barrier for the formation of the bcc PC from the fluid is lower than the nucleation barrier for the formation of the fcc PC from the fluid.[76]

The results of this work make it possible to plot for the first time the complete phase diagram of the TIP4P/2005 model. This is presented in Fig. 9(a). The model provides a qualitatively correct description of the phase diagram of wa-

ter (see the correct location of ices Ih to VI). It is seen that the two PCs dominate the phase diagram of the TIP4P/2005 model of water for temperatures above 400 K. The bcc PC to fcc PC transition presents a small negative slope. The slopes of the melting curves of the bcc PC and of the fcc PC are quite similar and relatively small compared to the slope in the melting curve of the rest of the ices. In fact we found a slope of the melting curve of the PC solids of about 100 bars/K at temperatures around 550 K. This slope is smaller than the slope found in the melting curve of ices Ih, III, V, VI, and VII. In Fig. 9 (lower panel) the phase diagrams of the TIP4P/2005 are presented when the bcc PC [Fig. 9(b)] or fcc plastic [Fig. 9(c)] are not considered. These are virtual phase diagrams since for the TIP4P/2005 the fcc PC or bcc PC do indeed exists and the true phase diagram of the model is that of the upper panel. The purpose of the diagram of the Fig. 9(c) is to show that the coexistence curve between ice VII and the bcc PC always presents a positive slope. In other words ice VII is always more dense than the bcc PC at a given temperature and pressure. This is not surprising since both phases present the same arrangement of oxygen atoms, but the localized character of the hydrogen bonds in ice VII provokes a higher density. We do not expect any change in the sign of the slope in the coexistence line between ice VII and the bcc PC. However, in Fig. 9(b) we see a change in slope in the transition between ice VII and the fcc PC. At low pressures ice VII is more dense than the fcc PC (the stronger hydrogen bonds in ice VII compensate the less efficient packing of molecules in the bcc arrangement). However the VII-fcc PC presents re-entrant behavior. In fact a high pressures the fcc PC is more dense than ice VII. This is further illustrated in Fig. 10(a) where the equation of state of ice VII and of the fcc PC at 300 K are shown, from pressures of about 70 000 to extremely high pressures. The crossing in the densities is clear. Notice that the crossing does not indicate any phase transition. The black filled circles in Fig. 10(a) indicate the coexistence point as obtained from Gibbs–Duhem simulations. At sufficiently high pressures the more efficient packing of the fcc arrangement of oxygens dominates the physics of the model. The density of the bcc PC is intermediate between that of the fluid and that of ice VII at the same T and p [Fig. 10(b)]. The physics of PC has been discussed before for simple models[77] such as hard diatomic molecules.[78–85]

Let us now analyze if the PC phases also appear in other water models such as TIP4P and SPC/E. Although we computed the phase diagram for these two models in our previous work[34] it seems necessary to recalculate the upper part of the phase diagram for at least two reasons. First because we did not consider the possibility of having plastic PC phases in the phase diagram. Second because the free energy calculations for ice VII were performed at a temperature and pressure where the system was already in a PC phase (443 K and a pressure of about 78 350 bars). Therefore our free energy calculations for ice VII (reported recently in Ref. 56) of the TIP4P and SPC/E were incorrect. The rest of free energies and coexistence lines are correct. By performing Hamiltonian Gibbs–Duhem integration we estimate an initial coexistence point for the coexistence lines involving ice VII and

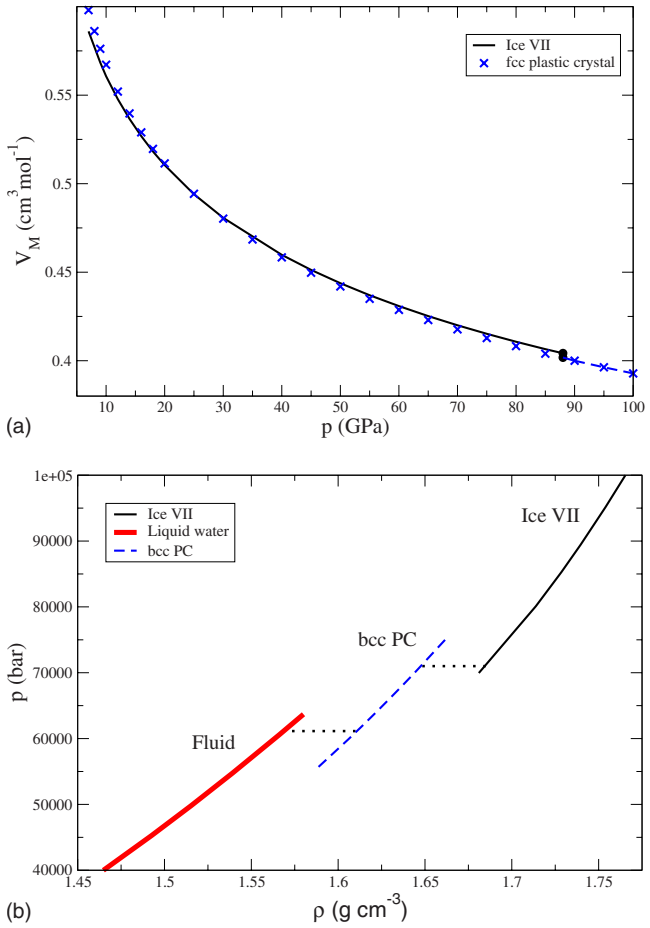

FIG. 10. (Color online) (a) Equation of state of ices VII (solid line) and fcc PC (crosses) for 300 K as obtained from computer simulation for TIP4P/2005 model. Lines indicate thermodynamic stable phase for each pressure. For low pressures the solid line corresponds to ice VII. At high pressures the dashed line with crosses corresponds to fcc PC. The coexistence point between the two ices is given by the filled circles. (b) Equation of state of ice VII (thin solid line), bcc PC (dashed line), and liquid water (thick solid line) for 380 K as obtained by computer simulation for TIP4P/2005 model. The dotted lines gives the coexistence.

the PC phases. Once this initial point was located the rest of the coexistence line was obtained by Gibbs–Duhem integration. The complete phase diagrams of TIP4P and SPC/E are presented in Fig. 11 along with the experimental phase diagram. The phase diagram for the TIP4P model is very similar to that of the TIP4P/2005 model but shifted to lower temperatures by about 20 K (this shift is found for instance in the melting point of ice Ih for these two models). The phase diagram of SPC/E is dominated by ice II (ice Ih appears at negative pressures and ices III and V disappear from the phase diagram). The pressure at the fluid-ice VI-ice VII triple point for TIP4P and SPC/E is now about 55 000 bars (compared to a value of about 85 000 bars reported in our previous work). This new location of the triple point is in better agreement with the experimental pressure at the triple point between ice VI, ice VII and the fluid (which is about 30 000 bars). The agreement is not yet quantitative though. It is clear that both PC phases appear in the phase diagram of these two water models. The main difference between SPC/E and TIP4P is the size of the stability region of the bcc PC (larger for the SPC/E). Notice also the change of slope of the ice

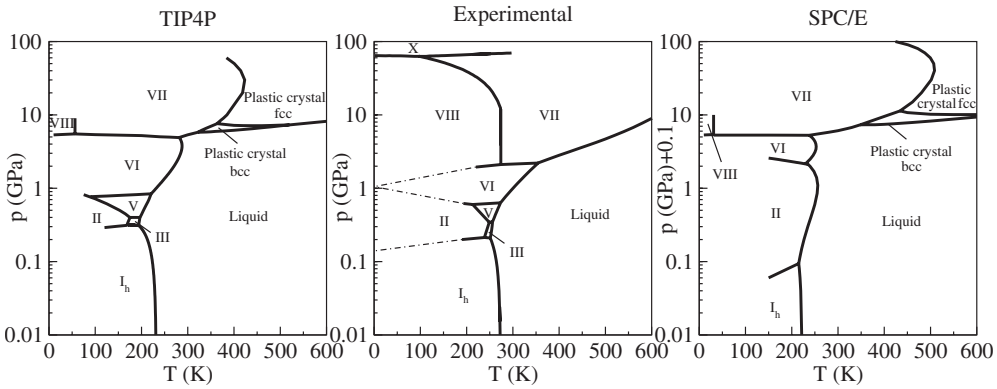

FIG. 11. Phase diagram of H_2O. Left: simulation results for the TIP4P model; right: simulation results for the SPC/E model; middle: experimental phase diagram. For the SPC/E the coexistence pressures have been shifted by 0.1 GPa to include results for the ice I (which appears for the SPC/E at slightly negative pressures). The Gibbs–Duhem coexistence lines for SPC/E and TIP4P models can be found as electronic supplementary information (Ref. 69) and Ref. 71.

VIII-ice VII transition observed in the experimental phase diagram. According to our previous discussion of the ice VII-fcc PC transition this change in the slope points to a greater density of the phase on the right (ice VII) with respect to the phase on the left (ice VIII). It has been suggested[48,13,86–89] that the hydrogens become dynamically disordered in ice VII between the two positions along the O–O lines and finally occupies the central location of the O–O lines in ice X. This could provoke a more dense packing in ice VII, explaining the negative slope of the experimental coexistence line between ices VIII and VII (although it would be interesting to know whether ice VIII is affected or not by a similar possible resonance and symmetrization of the hydrogens).

These PC phases have not been reported so far for real water. Schwager and Boehler[90] in a very recent experimental study suggests the existence of a new ice phase from 20 to 42 GPa. The structure of this new solid is unknown but the melting curve has been reported. In Fig. 12 the melting curve reported by Schwager *et al.* is plotted along with the melting curve of ice VII reported by several other groups. In Fig. 12(a) we present the upper part of the phase diagram of TIP4P/2005 as presented in Fig. 9(c) (i.e., when the fcc PC solid is not included). The similarity in the slopes between experiment and simulation is striking. In particular the slope of the melting curve reported by most of experimental groups seems to correspond to the ice VII-bcc PC obtained in computer simulations. However, the melting line reported by Schwager and Boehler[90] seems to correspond to the melting curve of the bcc PC obtained in simulations. Notice the small slope of the melting curve reported by Schwager and Boehler.[90] As discussed above the small slope of the melting curve is a signature of PC phases. In Fig. 12(b) we compare the fluid-fcc PC and VII-fcc PC coexistence lines as presented in Fig. 9(b) when the bcc PC solid is not included to the experimental measurements of the ice VII melting line. The fluid-fcc PC line is very similar to the melting curve reported by Schwager and Boehler,[90] whereas the slope of the VII-fcc PC coexistence line is similar to the rest of the experimental melting lines given for ice VII. The main difference is that there a change in slope in the transition between ice VII and the fcc PC. In view of this, it seems to be reasonable to think that the new phase reported by Schwager could be a PC phase (it is not clear what it could be, bcc PC

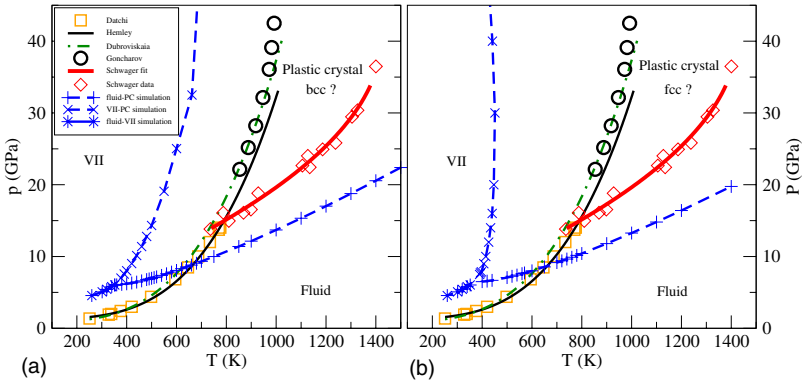

FIG. 12. (Color online) Experimental measurements of the ice VII melting curve. The open circles correspond to the Goncharov values Ref. 15, the dashed-dotted line is given by Dubronskaia and Dubrovinky (Ref. 16), the thin solid line corresponds to the Lin results (Ref. 17), the open squares is taken from Ref. 18, and the diamonds and the thick solid line are given by Schwanger *et al.* (Ref. 20). Right: The melting curve of the fcc PC obtained by simulations correspond to the dashed line with pluses, the simulated coexistence curve ice VII-fcc PC phase is the dashed line with crosses and the dashed line with stars correspond to the simulated melting line of the ice VII. Left: The melting curve of the bcc PC obtained by simulations correspond to the dashed line with pluses, the simulated coexistence curve ice VII-bcc PC phase is the dashed line with crosses and the dashed line with stars correspond to the simulated melting line of the ice VII.

or fcc PC). Obviously further work is needed to clarify this. The melting curve of Schwager and Boehler[90] increases its slope for temperatures above 1300 K. The sharp increase in the slope of the melting curve could be due to the presence of molecular dissociation and proton diffusion in the solid before melting (typical behavior of type-II superionic solids[47]). This cannot be reproduced using rigid nonpolarizable models and for this reason our simulations do not reproduce the sharp increase in the slope of the melting curve for temperatures greater than 1300 K.

IV. CONCLUSIONS

In this work the characterization and localization in the phase diagram of water of a new fcc PC phase has been performed by computer simulation by using the TIP4P/2005 model. This PC was obtained through a Martensitic transformation of the bcc PC. By performing free energy calculations it was further confirmed that it is thermodynamically stable at certain T and p. Details about how to perform free energy calculations for PC phases of water have been provided. Once the free energies for the fluid, ice VII and the two PC phases were determined it was possible to determine the upper pressure part of the phase diagram of TIP4P/2005. Melting points predicted by free energy calculations were further confirmed by direct coexistence techniques.

We have recalculated the high pressure region of the phase diagram for the TIP4P and SPC/E models using Hamiltonian Gibbs–Duhem integration. It has been shown that for all these water models these two PC phases appear in the upper region of the phase diagram. In fact for these water models the melting curves at high temperatures are dominated by the PC phases.

It would be of interest to study if such PC phases do indeed exist for real water. As has been seen, the bcc PC phase (or the fcc PC) could be the new ice phase reported by Schwager and Boehler.[90] The discrepancies between the melting curve given by Schwager and the rest of the experimental groups could be due to the fact that Schwager is determining the PC-fluid transition, whereas the other groups may be determining the ice VII-PC transformation. The presence of PC phases for real water would have consequences for the large community performing computer simulations of water. Its presence would indicate that current water models can still provide estimates of the behavior of water even at high pressures (provided that no dissociation of the molecules occurs). Its absence would also be significant since it would indicate that current water models are too spherical and they should be modified so as to predict the disappearance of the PC phases.

ACKNOWLEDGMENTS

This work was funded by Grant No. FIS2007-66079-C02-01 from the DGI (Spain), Grant No. S-0505/ESP/0299 from the CAM, and Grant No. 910570 from the UCM. J. L. Aragones would like to thank the MEC by the award of a predoctoral grant. Helpful discussions with L. G. MacDowell, J. L. F. Abascal, and E. G. Noya are gratefully acknowledged. We would like to thank Carl McBride for a critical reading.

[1] G. Tammann, *Kristallisieren und Schmelzen* (Johann Ambrosius Barth, Leipzig, 1903).
[2] G. Tammann, Z. Phys. Chem. **68**, 205 (1910).
[3] P. W. Bridgman, Proc. Am. Acad. Arts Sci. **47**, 441 (1912).
[4] C. Lobban, J. L. Finney, and W. F. Kuhs, Nature (London) **391**, 268 (1998).
[5] C. G. Salzmann, P. G. Radaelli, A. Hallbrucker, E. Mayer, and J. L. Finney, Science **311**, 1758 (2006).
[6] E. Whalley, D. W. Davidson, and J. B. R. Heath, J. Chem. Phys. **45**, 3976 (1966).
[7] S. Kawada, J. Phys. Soc. Jpn. **32**, 1442 (1972).
[8] E. Whalley, J. B. R. Heath, and D. W. Davidson, J. Chem. Phys. **48**, 2362 (1968).
[9] P. W. Bridgman, J. Chem. Phys. **5**, 964 (1937).
[10] A. F. Goncharov, V. V. Struzhkin, M. S. Somayazulu, R. J. Hemley, and H. K. Mao, Science **273**, 218 (1996).
[11] M. Somayazulu, J. Shu, C. Zha, A. F. Goncharov, O. Tschauner, H. Mao, and R. Hemley, J. Chem. Phys. **128**, 064510 (2008).
[12] W. F. Kuhs, J. L. Finney, C. Vettier, and D. V. Bliss, J. Chem. Phys. **81**, 3612 (1984).
[13] E. Wolanin, P. Pruzan, J. C. Chervin, B. Canny, M. Gauthier, D. Häusermann, and M. Hanfland, Phys. Rev. B **56**, 5781 (1997).
[14] C. R. Bina and A. Navrotsky, Nature (London) **408**, 844 (2000).
[15] A. Goncharov, N. Goldman, L. E. Fried, J. C. Crowhurst, I. W. Kuo, C. J. Mundy, and J. M. Zaug, Phys. Rev. Lett. **94**, 125508 (2005).
[16] N. Dubrovinskaia and L. Dubrovinky, High Press. Res. **23**, 307 (2003).
[17] J. Lin, B. Militzer, V. V. Struzhkin, E. Gregoryanz, R. Hemley, and H. Mao, J. Chem. Phys. **121**, 8423 (2004).
[18] F. Datchi, F. P. Loubeyre, and R. LeToullec, Phys. Rev. B **61**, 6535 (2000).
[19] O. Mishima and S. Endo, J. Chem. Phys. **68**, 4417 (1978).
[20] B. Schwager, L. Chudinovskikh, A. Gavriliuk, and R. Boehler, J. Phys.: Condens. Matter **16**, S1177 (2004).
[21] G. P. Johari, A. Lavergne, and E. Whalley, J. Chem. Phys. **61**, 4292 (1974).
[22] C. W. F. T. Pistorius, E. Rapoport, and J. B. Clark, J. Chem. Phys. **48**, 5509 (1968).
[23] J. A. Barker and R. O. Watts, Chem. Phys. Lett. **3**, 144 (1969).
[24] A. Rahman and F. H. Stillinger, J. Chem. Phys. **55**, 3336 (1971).
[25] G. C. Boulougouris, J. R. Errington, I. G. Economou, A. Z. Panagiotopoulos, and D. N. Theodorou, J. Phys. Chem. B **104**, 4958 (2000).
[26] M. Lisal, W. R. Smith, and I. Nezbeda, Fluid Phase Equilib. **181**, 127 (2001).
[27] I. F. W. Kuo, C. J. Mundy, B. L. Eggimann, M. J. McGrath, J. I. Siepmann, B. Chen, J. Vieceli, and D. J. Tobias, J. Phys. Chem. B **110**, 3738 (2006).
[28] G. T. Gao, X. C. Zeng, and H. Tanaka, J. Chem. Phys. **112**, 8534 (2000).
[29] Y. Koyama, H. Tanaka, G. Gao, and X. C. Zeng, J. Chem. Phys. **121**, 7926 (2004).
[30] H. Nada and J. P. J. M. van der Eerden, J. Chem. Phys. **118**, 7401 (2003).
[31] M. J. Vlot, J. Huinink, and J. P. van der Eerden, J. Chem. Phys. **110**, 55 (1999).
[32] O. A. Karim and A. D. J. Haymet, J. Chem. Phys. **89**, 6889 (1988).
[33] B. F. Nicholson, P. Clancy, and S. W. Rick, J. Cryst. Growth **293**, 78 (2006).
[34] E. Sanz, C. Vega, J. L. F. Abascal, and L. G. MacDowell, Phys. Rev. Lett. **92**, 255701 (2004).
[35] H. J. C. Berendsen, J. R. Grigera, and T. P. Straatsma, J. Phys. Chem. **91**, 6269 (1987).
[36] W. L. Jorgensen, J. Chandrasekhar, J. D. Madura, R. W. Impey, and M. L. Klein, J. Chem. Phys. **79**, 926 (1983).
[37] J. L. F. Abascal and C. Vega, J. Chem. Phys. **123**, 234505 (2005).
[38] C. Vega, J. L. F. Abascal, M. M. Conde, and J. L. Aragones, Faraday Discuss. **141**, 251 (2009).
[39] D. H. Dolan, M. D. Knudson, C. A. Hall, and C. Deeney, Nat. Phys. **3**, 339 (2007).
[40] J. L. Aragones, M. M. Conde, E. G. Noya, and C. Vega, Phys. Chem. Chem. Phys. **11**, 543 (2009).
[41] M. Matsumoto, S. Saito, and I. Ohmine, Nature (London) **416**, 409 (2002).
[42] D. Quigley and P. M. Rodger, J. Chem. Phys. **128**, 154518 (2008).

[43] L. Vrbka and P. Jungwirth, J. Phys. Chem. B **110**, 18126 (2006).
[44] I. Svishchev and P. G. Kusalik, Phys. Rev. Lett. **73**, 975 (1994).
[45] Y. Takii, K. Koga, and H. Tanaka, J. Chem. Phys. **128**, 204501 (2008).
[46] D. A. Young, *Phase Diagram of the Elements* (University of California, California, 1991).
[47] E. Schwegler, M. Sharma, F. Gygi, and G. Galli, Proc. Natl. Acad. Sci. U.S.A. **105**, 14779 (2008).
[48] M. Benoit, D. Marx, and M. Parrinello, Nature (London) **392**, 258 (1998).
[49] M. Parrinello and A. Rahman, J. Appl. Phys. **52**, 7182 (1981).
[50] S. Yashonath and C. N. R. Rao, Mol. Phys. **54**, 245 (1985).
[51] S. Nosé and M. L. Klein, Mol. Phys. **50**, 1055 (1983).
[52] D. Frenkel and A. J. C. Ladd, J. Chem. Phys. **81**, 3188 (1984).
[53] J. M. Polson, E. Trizac, S. Pronk, and D. Frenkel, J. Chem. Phys. **112**, 5339 (2000).
[54] P. A. Monson and D. A. Kofke, in *Advances in Chemical Physics*, edited by I. Prigogine and S. A. Rice (Wiley, New York, 2000), Vol. 115, p. 113.
[55] C. Vega and E. G. Noya, J. Chem. Phys. **127**, 154113 (2007).
[56] C. Vega, E. Sanz, E. G. Noya, and J. L. F. Abascal, J. Phys.: Condens. Matter **20**, 153101 (2008).
[57] E. G. Noya, M. M. Conde, and C. Vega, J. Chem. Phys. **129**, 104704 (2008).
[58] G. E. Lindberg and F. Wang, J. Phys. Chem. B **112**, 6436 (2008).
[59] D. Frenkel and B. Smit, *Understanding Molecular Simulation* (Academic, London, 1996).
[60] D. A. Kofke, J. Chem. Phys. **98**, 4149 (1993).
[61] D. A. Kofke, in *Monte Carlo Methods in Chemical Physics*, edited by D. M. Ferguson, J. I. Siepmann, and D. G. Truhlar (Wiley, New York, 1998), Vol. 105, p. 405.
[62] D. V. der Spoel, E. Lindahl, B. Hess, G. Groenhof, A. E. Mark, and H. J. C. Berendsen, J. Comput. Chem. **26**, 1701 (2005).
[63] S. Nosé, Mol. Phys. **52**, 255 (1984).
[64] W. G. Hoover, Phys. Rev. A **31**, 1695 (1985).
[65] U. Essmann, L. Perera, M. L. Berkowitz, T. Darden, H. Lee, and L. G. Pedersen, J. Chem. Phys. **103**, 8577 (1995).
[66] N. B. Wilding, Mol. Phys. **107**, 295 (2009).
[67] J. D. Lee and H. W. Pakes, Acta Crystallogr., Sect. A: Cryst. Phys., Diffr., Theor. Gen. Crystallogr. **25**, 712 (1969).
[68] L. Pusztai, O. Pizio, and S. Sokolowski, J. Chem. Phys. **129**, 184103 (2008).
[69] See EPAPS supplementary material at http://dx.doi.org/10.1063/1.3156856 for MD trajectories of the ice VII, bcc PC and fcc PC in mpg format and coexistence lines of the SPC/E and TIP4P models for the high pressure polymorphs (ice VII, bcc PC and fcc PC) and fluid as obtained by Gibbs-Duhem integration.
[70] E. de Miguel, R. G. Marguta, and E. M. del Rio, J. Chem. Phys. **127**, 154512 (2007).
[71] J. L. F. Abascal, E. Sanz, and C. Vega, Phys. Chem. Chem. Phys. **11**, 556 (2009).
[72] A. J. C. Ladd and L. Woodcock, Chem. Phys. Lett. **51**, 155 (1977).
[73] A. J. C. Ladd and L. Woodcock, Mol. Phys. **36**, 611 (1978).
[74] J. Cape and L. Woodcock, Chem. Phys. Lett. **59**, 271 (1977).
[75] D. H. Dolan, J. N. Johnson, and Y. M. Gupta, J. Chem. Phys. **123**, 64702 (2005).
[76] W. Ostwald, Z. Phys. Chem. **22**, 289 (1897).
[77] D. Frenkel and B. M. Mulder, Mol. Phys. **55**, 1171 (1985).
[78] C. Vega and P. A. Monson, J. Chem. Phys. **107**, 2696 (1997).
[79] C. Vega, E. P. A. Paras, and P. A. Monson, J. Chem. Phys. **97**, 8543 (1992).
[80] C. Vega, E. P. A. Paras, and P. A. Monson, J. Chem. Phys. **96**, 9060 (1992).
[81] E. P. A. Paras, C. Vega, and P. A. Monson, Mol. Phys. **77**, 803 (1992).
[82] E. P. A. Paras, C. Vega, and P. A. Monson, Mol. Phys. **79**, 1063 (1993).
[83] C. Vega and P. A. Monson, J. Chem. Phys. **102**, 1361 (1995).
[84] S. J. Singer and R. Mumaugh, J. Chem. Phys. **93**, 1278 (1990).
[85] M. Marechal and M. Dijkstra, Phys. Rev. E **77**, 061405 (2008).
[86] R. J. Hemley, A. P. Jephcoat, H. K. Mao, C. S. Zha, L. W. Finger, and D. E. Cox, Nature (London) **330**, 737 (1987).
[87] P. Loubeyre, R. LeToullec, E. Wolanin, M. Hanfland, and D. Hausermann, Nature (London) **397**, 503 (1999).
[88] E. Sugimura, Y. Iitaka, K. Hirose, K. Kawamura, N. Sata, and Y. Ohishi, Phys. Rev. B **77**, 214103 (2008).
[89] M. Benoit, M. Bernasconi, P. Focher, and M. Parrinello, Phys. Rev. Lett. **76**, 2934 (1996).
[90] B. Schwager and R. Boehler, High Press. Res. **28**, 431 (2008).